VII International Conference on Computational Plasticity
COMPLAS 2003
E. Oñate and D. R. J. Owen (Eds)

INELASTIC DYNAMIC ANALYSIS OF SHELLS WITH THE TRIC SHELL ELEMENT

M. Papadrakakis[*], Z. S. Mouroutis[*], L. Karapitta[*] and A.G. Papachristidis[*,†]

[*] Institute of Structural Analysis & Seismic Research
National Technical University Athens, Zografou Campus, Athens 15780, Greece
e-mail: {mpapadra,zachmour,klucia}@central.ntua.gr

[†] 4M – VK Civil Engineering Software Inc.
Mykinon 9 & Kifisias, GR-15233 Athens, Greece
Email: aris@4m.gr, web page: http://www.4m.gr

Key words: Inelastic, dynamic, shells, TRIC.

Abstract. *The dynamic analysis of shells has attracted considerable interest in recent years. As analysts are increasingly performing more sophisticated simulations of complex structural models (some problems may comprise hundreds of thousands or even millions degrees of freedom) there is a great need for simple, and at the same time, accurate elements to conduct large-scale computational experiments. Furthermore, most available shell elements lack generality, that is, they are either isotropic or composite. In addition there is a trend in finite element analysis for numerical integration that calls for stiffness and mass matrices containing analytic algebraic expressions. To satisfy these requirements, a lot effort has been devoted to expand and further develop the natural mode finite element method for the analysis of isotropic and laminated composite shell structures. The product of this effort is the TRIC (TRIangular Composite) element, which has been presented in previous papers. The aim of this work is to present the behavior of the TRIC element in geometrical as well as nonlinear dynamic analysis of shells.*

1 INTRODUCTION

When faced with the challenge of investigating time-dependent nonlinear phenomena of shell structures with the finite element method a major constraint arises which is the high computational cost involved in the simulations. Higher order shell elements have been successfully proposed in the past for linear analysis. However, the extension of this type of shell elements to the nonlinear range and especially to time-dependent problems is not straightforward. Isoparametric finite elements based on higher-order interpolation functions and multiple quadrature loops can prove very expensive and cumbersome when applied to large and complex multilayered shells.

Hence, the development of a simple plate and shell finite element including transverse shear deformation, capable of engineering accuracy, competent in the study of intricate nonlinear phenomena and adaptable to many types of material systems including isotropic, sandwich, laminated, composite and hybrid structures remains a challenging task. A shell finite element that has been proved to have all the above-mentioned characteristics in static linear and nonlinear problems is the TRIC shell element initiated by J. Argyris and further developed in a number of subsequent papers[i,ii,iii,iv,v].

The aim of this paper is to formulate a consistent mass matrix that includes both translational and rotational inertia in order to test the efficiency of the TRIC element in linear and materially nonlinear dynamic problems.

2 THE PRINCIPAL OF VIRTUAL WORK IN DYNAMICS

All the implicit time integration schemes developed for linear dynamic analysis can also be applied to nonlinear dynamic response calculations. Using, for example, the Newton Raphson iteration and neglecting the effects of a damping matrix, the governing dynamic equilibrium equation is:

$$\mathbf{M}\,{}^{t+\Delta t}\ddot{\mathbf{U}}^{(k+1)} + {}^{t+\Delta t}\mathbf{K}^{(k)}\Delta\mathbf{U}^{(k+1)} = {}^{t+\Delta t}\mathbf{R} - {}^{t+\Delta t}\mathbf{F}^{(k)} \tag{1}$$

where k, k+1 represent the iterations within the time step Δt. With the Newmark approximations:

$${}^{t+\Delta t}\ddot{\mathbf{U}} = \frac{1}{\beta\Delta t^2}\left({}^{t+\Delta t}\mathbf{U} - {}^{t}\mathbf{U}\right) - \frac{1}{\beta\Delta t}\cdot{}^{t}\dot{\mathbf{U}} - \frac{1}{2\beta}{}^{t}\ddot{\mathbf{U}} + {}^{t}\ddot{\mathbf{U}} \tag{2}$$

and introducing iterations k, k+1 within the time step

$${}^{t+\Delta t}\ddot{\mathbf{U}}^{(k+1)} = \frac{1}{\beta\Delta t^2}\left({}^{t+\Delta t}\mathbf{U}^{(k)} - {}^{t}\mathbf{U} + \Delta\mathbf{U}^{(k+1)}\right) - \frac{1}{\beta\Delta t}\cdot{}^{t}\dot{\mathbf{U}} - \frac{1}{2\beta}{}^{t}\ddot{\mathbf{U}} + {}^{t}\ddot{\mathbf{U}} \tag{3}$$

Eq. (1) becomes:

$$\left({}^{t+\Delta t}\mathbf{K}^{(k)} + \frac{\mathbf{M}}{\beta\Delta t^2}\right)\Delta\mathbf{U}^{(k+1)} = {}^{t+\Delta t}\mathbf{R} - {}^{t+\Delta t}\mathbf{F}^{(k)} - \mathbf{M}\left\{\frac{1}{\beta\Delta t^2}\left({}^{t+\Delta t}\mathbf{U}^{(k)} - {}^{t+\Delta t}\mathbf{U}\right) - \frac{1}{\beta\Delta t}{}^{t}\dot{\mathbf{U}} - \left(\frac{1}{2\beta} - 1\right){}^{t}\ddot{\mathbf{U}}\right\} \tag{4}$$

which can be solved for the incremental displacements at iteration k+1 inside the time steps.

3 THE MASS MATRIX

The computation of the consistent elemental mass matrix necesitates the estimation of matrix $\boldsymbol{\omega}$ containing the modal functions. More specifically, the displacement vector $\boldsymbol{u}$ must be expressed as a function of the natural modes. Then the global elemental mass matrix can be established via:

$$\underset{(18x18)}{M_e} = \underset{(18x18)}{a^T} \left(\int_{V_e} \rho \underset{(18x3)}{\omega^T} \underset{(3x18)}{\omega} dV \right) \underset{(18x18)}{a} \tag{5}$$

where $\boldsymbol{\alpha}$ is the transformation matrix from the local natural coordinate system of each element to the global Cartesian coordinate system and ρ is the density of the material.

The modal matrix $\boldsymbol{\omega}$ can be derived by invoking kinematic and geometric arguments. Similarly to static analysis, the rotational inertia forces resulting from antisymmetric deformation are assumed uncoupled from the other forces, and as such they are treated independently. The derivation of the part of the modal matrix that contains the rigid body modes is straightforward [i] and it can be graphically depicted in Figure 1.

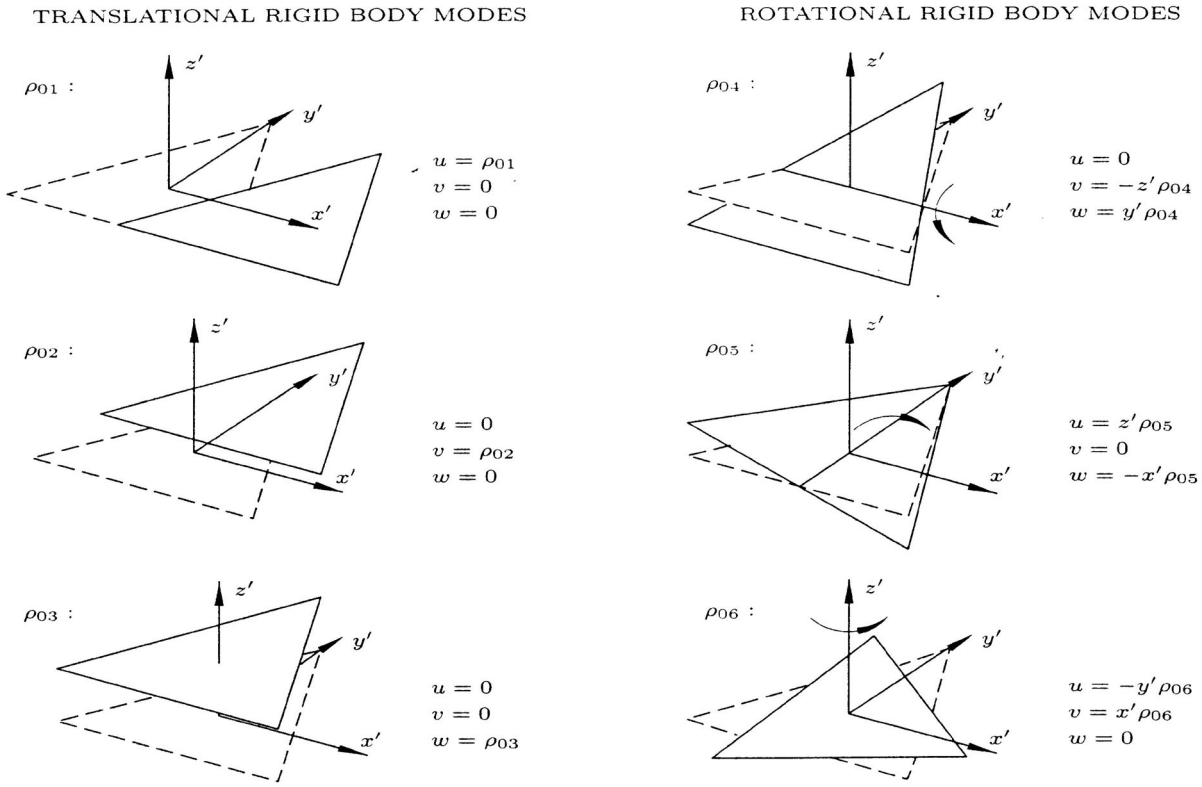

Figure 1: Rigid body modes

The second component of the modal matrix is related to the axial straining modes ($\gamma_{t\alpha}$, $\gamma_{t\beta}$ and $\gamma_{t\gamma}$) along the sides of the triangular element. From Figure 2, it can be concluded that the displacements of node Γ, for example, are given by:

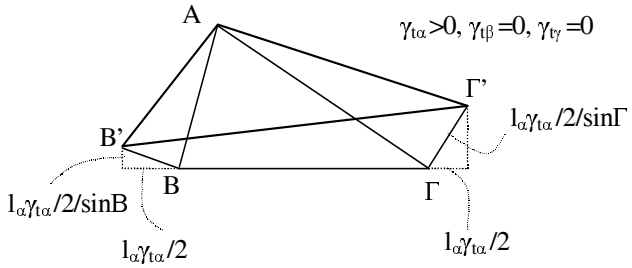

Figure 2: Axial straining mode $\gamma_{t\alpha}$

$$u_3 = \frac{l_a}{2\sin\Gamma}\cos\left(\beta - \frac{\pi}{2}\right)\gamma_{ta} + \frac{l_\beta}{2\sin\Gamma}\cos\left(a - \frac{\pi}{2}\right)\gamma_{t\beta} \tag{6}$$

$$v_3 = \frac{l_a}{2\sin\Gamma}\sin\left(\beta - \frac{\pi}{2}\right)\gamma_{ta} + \frac{l_\beta}{2\sin\Gamma}\sin\left(a - \frac{\pi}{2}\right)\gamma_{t\beta} \tag{7}$$

or:

$$u_3 = \frac{l_a \sin\beta}{2\sin\Gamma}\gamma_{ta} + \frac{l_\beta \sin\alpha}{2\sin\Gamma}\gamma_{t\beta} \tag{8}$$

$$v_3 = -\frac{l_a \cos\beta}{2\sin\Gamma}\gamma_{ta} - \frac{l_\beta \cos\alpha}{2\sin\Gamma}\gamma_{t\beta} \tag{9}$$

and finally:

$$u_3 = \frac{l_\alpha^2 y_\beta}{4\Omega}\gamma_{ta} + \frac{l_\beta^2 y_\alpha}{4\Omega}\gamma_{t\beta} \tag{10}$$

$$v_3 = -\frac{l_\alpha^2 x_\beta}{4\Omega}\gamma_{ta} - \frac{l_\beta^2 x_\alpha}{4\Omega}\gamma_{t\beta} \tag{11}$$

Similar expressions can be derived for the other two nodes leading to the following expressions for the inplane displacements of the element due to the axial straining modes along the side of the triangle:

$$u = \frac{l_\alpha^2}{4\Omega}\left(y_\gamma\zeta_\beta + y_\beta\zeta_\gamma\right)\gamma_{ta} + \frac{l_\beta^2}{4\Omega}\left(y_\alpha\zeta_\gamma + y_\gamma\zeta_\alpha\right)\gamma_{t\beta} + \frac{l_\gamma^2}{4\Omega}\left(y_\alpha\zeta_\beta + y_\beta\zeta_\alpha\right)\gamma_{t\gamma} \tag{12}$$

$$v = -\frac{l_\alpha^2}{4\Omega}\left(x_\gamma\zeta_\beta + x_\beta\zeta_\gamma\right)\gamma_{ta} - \frac{l_\beta^2}{4\Omega}\left(x_\alpha\zeta_\gamma + x_\gamma\zeta_\alpha\right)\gamma_{t\beta} - \frac{l_\gamma^2}{4\Omega}\left(x_\alpha\zeta_\beta + x_\beta\zeta_\alpha\right)\gamma_{t\gamma} \tag{13}$$

where ζ_α, ζ_β, ζ_γ, are the area coordinates of the triangular element. By setting any of the axial straining modes equal to 1 and the others equal to zero the corresponding modal functions can be obtained.

For the derivation of the expressions of the symmetric and antisymmetric modal functions, the following expression of the vertical (out of the plane) displacement is used[iv]:

$$\begin{aligned} w = &\frac{1}{2}l_\alpha\zeta_\beta\zeta_\gamma\psi_{s\alpha} + \frac{1}{2}l_\beta\zeta_\alpha\zeta_\gamma\psi_{s\beta} + \frac{1}{2}l_\gamma\zeta_\alpha\zeta_\beta\psi_{s\gamma} + \frac{1}{2}l_\alpha\zeta_\beta\zeta_\gamma\left(\zeta_\beta - \zeta_\gamma\right)\psi_{A\alpha} + \\ &\frac{1}{2}l_\beta\zeta_\alpha\zeta_\gamma\left(\zeta_\gamma - \zeta_\alpha\right)\psi_{A\beta} + \frac{1}{2}l_\gamma\zeta_\alpha\zeta_\beta\left(\zeta_\alpha - \zeta_\beta\right)\psi_{A\gamma} \end{aligned} \tag{14}$$

where $\psi_{s\alpha}$, $\psi_{s\beta}$ and $\psi_{s\gamma}$ are the natural symmetric bending modes and $\psi_{A\alpha}$, $\psi_{A\beta}$ and $\psi_{A\gamma}$ are the natural antisymmetric bending modes. Thus, for example, for $\psi_{s\alpha}$=1 and all the other modes equal to 0 Eq. (14) becomes:

$$w = \frac{1}{2}l_\alpha\zeta_\beta\zeta_\gamma \tag{15}$$

Since:

$$u = -z\,\partial w/\partial x = -z\left(\frac{\partial w}{\partial\zeta_\alpha}\frac{\partial\zeta_\alpha}{\partial x} + \frac{\partial w}{\partial\zeta_\beta}\frac{\partial\zeta_\beta}{\partial x} + \frac{\partial w}{\partial\zeta_\gamma}\frac{\partial\zeta_\gamma}{\partial x}\right) \tag{16}$$

$$v = -z\,\partial w/\partial y = -z\left(\frac{\partial w}{\partial\zeta_\alpha}\frac{\partial\zeta_\alpha}{\partial y} + \frac{\partial w}{\partial\zeta_\beta}\frac{\partial\zeta_\beta}{\partial y} + \frac{\partial w}{\partial\zeta_\gamma}\frac{\partial\zeta_\gamma}{\partial y}\right) \tag{17}$$

the expressions for u, v become:

$$\begin{aligned} u &= \frac{zl_\alpha}{4\Omega}\left(y_\beta\zeta_\gamma + y_\gamma\zeta_\beta\right) \\ v &= -\frac{zl_\alpha}{4\Omega}\left(x_\beta\zeta_\gamma + x_\gamma\zeta_\beta\right) \end{aligned} \tag{18}$$

In a similar way, the expressions of the other symmetric and antisymmetric modal functions can be deduced. Finally, the expressions for the natural azimuth modes[i] are graphically depicted in Figure 3.

Symbolic computation is employed in order to carry out, in a clear way, the tedious but otherwise straightforward matrix multiplications of Equation 1. Consequently, all integrals are evaluated in an exact manner using the formula:

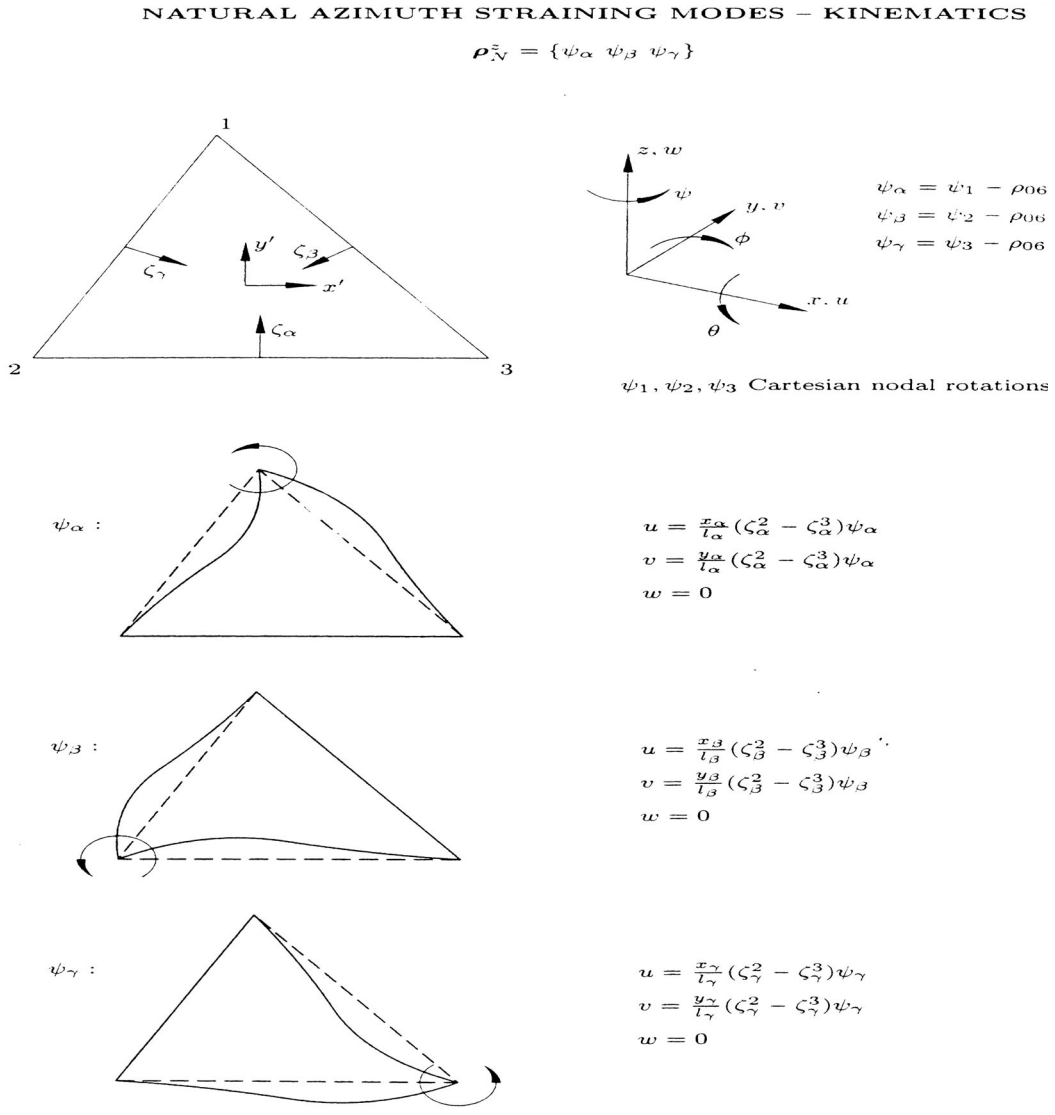

Figure 3: Azimuth straining modes

$$\frac{1}{\Omega}\int_{\Omega} \zeta_a^{\,p} \zeta_\beta^{\,q} \zeta_\gamma^{\,r} d\Omega = \frac{2!\,p!q!r!}{(2+p+q+r)!} \tag{19}$$

3 THE INELASTIC STIFFNESS MATRIX

The formulation of the stiffness matrix of the TRIC shell element has been analytically presented in previous papers[ii,iii,v]. In order to include a kinematic hardening effect in an elastoplastic model with a von Mises yield criterion, the yield function can be simply written by replacing the natural stress $\boldsymbol{\sigma}_c^i$ with $\xi_c^i = \boldsymbol{\sigma}_c^i - \boldsymbol{\alpha}_c^i$. The stress $\boldsymbol{\alpha}_c^i$ is known as back stress

and describes the translation of the center of the yield surface in stress space. A linear Ziegler's hardening law is adopted in this study, where

$$\dot{\boldsymbol{\alpha}}_c^i = \frac{C}{\sigma_y^0}(\boldsymbol{\sigma}_c^i - \boldsymbol{\alpha}_c^i)\mathrm{d}\bar{\gamma}_t^{pl} \tag{20}$$

C is the kinematic hardening modulus, σ_y^0 is the yield stress and $\mathrm{d}\bar{\gamma}_t^{pl}$ is the incremental equivalent plastic strain.

The integration of flow rules and hardening parameters over an iteration step i using implicit backward Euler algorithm results in the following system of nonlinear equations:

$$\begin{aligned} G(\boldsymbol{\sigma}_c, \mathrm{d}\bar{\gamma}_t^{pl}) &= \left[\boldsymbol{\kappa}_{ct}^{el}\right]^{-1}\left[(\boldsymbol{\sigma}_c)^i - (\boldsymbol{\sigma}_c^{el})^i\right] + (\mathrm{d}\bar{\gamma}_t^{pl})^i \left.\frac{\partial \mathrm{F}(\boldsymbol{\sigma}_c, \bar{\gamma}_t^{pl})}{\partial \boldsymbol{\sigma}_c}\right|_i = \mathbf{0} \\ \mathrm{F}(\xi_c, \mathrm{d}\bar{\gamma}_t^{pl})^i &= \bar{\sigma} - \sigma_y = \left[\frac{3}{2}(\xi_c^t)^i\left[\mathbf{A} - \frac{1}{3}\mathbf{E}_3\right](\xi_c)^i\right]^{1/2} - \sigma_y^0 = 0 \end{aligned} \tag{21}$$

where σc is the natural stress vector, $\boldsymbol{\kappa}_{ct}^{el}$ is the elastic constitutive matrix, $\boldsymbol{\sigma}_c^{el}$ is the elastic predictor and $\bar{\sigma}$ the equivalent stress.

The unknowns of the system are the components of natural stress vector $\boldsymbol{\sigma}_c$ and the equivalent plastic strain $\bar{\gamma}_t^{pl}$. The system can be solved with the Newton Raphson method where as starting point is taken the elastic predictor $\boldsymbol{\sigma}_c^{el}$ and zero incremental equivalent plastic strain. The nonlinear problem is then linearized in a sequence of iterations until convergence:

$$\begin{aligned} \begin{bmatrix} \boldsymbol{\sigma}_c \\ \mathrm{d}\bar{\gamma}_t^{pl} \end{bmatrix}_i &= \begin{bmatrix} \boldsymbol{\sigma}_c \\ \mathrm{d}\bar{\gamma}_t^{pl} \end{bmatrix}_{i-1} - \left[\mathbf{J}_i\right]^{-1}\begin{bmatrix} G \\ F \end{bmatrix}_{i-1} \\ &= \begin{bmatrix} \boldsymbol{\sigma}_c \\ \mathrm{d}\bar{\gamma}_t^{pl} \end{bmatrix}_{i-1} - \begin{bmatrix} \frac{\partial G}{\partial \boldsymbol{\sigma}_c} & \frac{\partial G}{\partial \mathrm{d}\bar{\gamma}_t^{pl}} \\ \frac{\partial F}{\partial \boldsymbol{\sigma}_c} & \frac{\partial F}{\partial \mathrm{d}\bar{\gamma}_t^{pl}} \end{bmatrix}_i^{-1}\begin{bmatrix} G \\ F \end{bmatrix}_{i-1} = 0 \end{aligned} \tag{22}$$

The Jacobian **J** is given explicitly by

$$\mathbf{J}_i = \begin{bmatrix} \left[\boldsymbol{\kappa}_{ct}^{el}\right]^{-1} + \mathrm{d}\bar{\gamma}^{pl}\frac{\partial^2 \mathrm{F}(\xi_c, \mathrm{d}\bar{\gamma}_t^{pl})}{\partial \boldsymbol{\sigma}_c^{\,2}} & \frac{\partial F(\xi_c, \mathrm{d}\bar{\gamma}_t^{pl})}{\partial \boldsymbol{\sigma}_c} + \mathrm{d}\bar{\gamma}^{pl}\frac{\partial^2 \mathrm{F}(\xi_c, \mathrm{d}\bar{\gamma}_t^{pl})}{\partial \boldsymbol{\sigma}_c \partial \mathrm{d}\bar{\gamma}^{pl}} \\ \left(\frac{\partial \mathrm{F}(\xi_c, \mathrm{d}\bar{\gamma}_t^{pl})}{\partial \boldsymbol{\sigma}_c}\right)^t & \frac{\partial \mathrm{F}(\xi_c, \mathrm{d}\bar{\gamma}_t^{pl})}{\partial \mathrm{d}\bar{\gamma}^{pl}} \end{bmatrix}_i \tag{23}$$

where

$$\frac{\partial F(\xi_c, d\bar{\gamma}_t^{pl})}{\partial \boldsymbol{\sigma}_c} = \frac{\partial F(\xi_c, d\bar{\gamma}_t^{pl})}{\partial \xi_c}\frac{\partial \xi_c}{\partial \boldsymbol{\sigma}_c} = \frac{3}{2}\frac{1}{\bar{\sigma}}\left[\mathbf{A} - \frac{1}{3}\mathbf{E}_3\right]\xi_c \tag{24}$$

$$\frac{\partial F(\xi_c, d\bar{\gamma}_t^{pl})}{\partial d\bar{\gamma}_t^{pl}} = \frac{\partial F(\xi_c, d\bar{\gamma}_t^{pl})}{\partial \xi_c}\frac{\partial \xi_c}{\partial \mathbf{a}_c}\frac{\partial \mathbf{a}_c}{\partial d\bar{\gamma}_t^{pl}} = -\frac{C}{\sigma_y^0}\bar{\sigma} = -\frac{C}{\sigma_y^0}\frac{3}{2}\frac{1}{\bar{\sigma}}\left[\mathbf{A} - \frac{1}{3}\mathbf{E}_3\right]\xi_c \tag{25}$$

$$\frac{\partial F^2(\boldsymbol{\sigma}_c, d\bar{\gamma}_t^{pl})}{\partial \boldsymbol{\sigma}_c \partial d\bar{\gamma}_t^{pl}} = -\frac{\partial F^2(\boldsymbol{\sigma}_c, d\bar{\gamma}_t^{pl})}{\partial \boldsymbol{\sigma}_c{}^2}\frac{C}{\sigma_y^0}\xi_c \tag{26}$$

$$\frac{\partial^2 F(\xi_c, d\bar{\gamma}_t^{pl})}{\partial \boldsymbol{\sigma}_c{}^2} = \frac{3}{2}\frac{1}{\bar{\sigma}}\left[\mathbf{A} - \frac{1}{3}\mathbf{E}_3\right] - \frac{9}{4}\frac{1}{\bar{\sigma}^3}\left[\mathbf{A} - \frac{1}{3}\mathbf{E}_3\right]\xi_c\xi_c{}^t\left[\mathbf{A} - \frac{1}{3}\mathbf{E}_3\right] \tag{27}$$

while $\left[\mathbf{A} - \frac{1}{3}\mathbf{E}_3\right]$ and $\bar{\sigma}$ are given in explicitly in reference (v). Once the components of natural stress and the equivalent plastic strain increment have been found, then all variables are defined at the end of the current iteration.

Alternatively the Eqs. (22) can be written as

$$\mathbf{J}\begin{bmatrix} d\boldsymbol{\sigma}_c \\ d\bar{\gamma}_t^{pl} \end{bmatrix} = \begin{bmatrix} \mathbf{J}_{n_\sigma x\, n_\sigma} & \mathbf{J}_{n_\sigma x\, n_{\bar{\gamma}}} \\ \mathbf{J}_{n_{\bar{\gamma}} x\, n_\sigma} & \mathbf{J}_{n_{\bar{\gamma}} x\, n_{\bar{\gamma}}} \end{bmatrix}\begin{bmatrix} d\boldsymbol{\sigma}_c \\ d\bar{\gamma}_t^{pl} \end{bmatrix} = \begin{bmatrix} d\gamma_t \\ 0 \end{bmatrix} \tag{28}$$

where $\mathbf{J}$ is the Jacobian calculated previously (Eq. (23)) and n_σ is the number of components of the stress natural vector while $n_{\bar{\gamma}}$ is in general the number of other unknowns variables that return mapping algorithm contains. In our case n_σ is equals to 3 and $n_{\bar{\gamma}}$ is equal to 1. Then the consistence tangent stiffness matrix is simply obtained as

$$\left[\boldsymbol{\kappa}_{ct}^{el-pl}\right]_i = \left.\frac{d\boldsymbol{\sigma}_c}{d\gamma_t}\right|_i = (\mathbf{J}_{n_\sigma x\, n_\sigma})_i^{-1} \tag{29}$$

where $(\mathbf{J}_{n_\sigma x\, n_\sigma})^{-1}$ is the inverse of the top left n_σ x n_σ submatrix of Jacobian $\mathbf{J}$.

The tangential stiffness matrix

Following the derivation of the tangent stiffness matrix[ii,iii] for geometric nonlinearities, the corresponding element tangent stiffness for large displacement, small strain and elasto-plastic material behaviour is given by the following expression[ii,iii]

$$\begin{aligned} \mathbf{k}_T &= [\mathbf{T}_{06}^t[\bar{\boldsymbol{\alpha}}_N^t[\mathbf{k}_N^{el-pl}]\bar{\boldsymbol{\alpha}}_N]\mathbf{T}_{06}] + [\mathbf{T}_{06}^t\bar{\mathbf{k}}_G\mathbf{T}_{06}] + [\mathbf{T}_{06}^t[\bar{\boldsymbol{\alpha}}_N^t[\mathbf{k}_{NG}]\bar{\boldsymbol{\alpha}}_N]\mathbf{T}_{06}] \\ &= \mathbf{T}_{06}^t\mathbf{k}_{LT}\mathbf{T}_{06} \end{aligned} \tag{30}$$

This expression reveals the main advantage of the present natural mode formulation: The

local elastic-plastic stiffness matrix $\overline{\boldsymbol{\alpha}}_{\mathrm{N}}^{\mathrm{t}}\mathbf{k}_{\mathrm{N}}^{\mathrm{el-pl}}\overline{\boldsymbol{\alpha}}_{\mathrm{N}}$ along with $\overline{\boldsymbol{\alpha}}_{\mathrm{N}}^{\mathrm{t}}\mathbf{k}_{\mathrm{NG}}\overline{\boldsymbol{\alpha}}_{\mathrm{N}}$ can be expressed analytically. These elemental components are added together to form the local tangent stiffness matrix $\mathbf{k}_{LT}$ at element level. Thus, only matrix multiplications $\mathbf{T}_{06}^{\mathrm{t}}\mathbf{k}_{\mathrm{LT}}\mathbf{T}_{06}$, with $\mathbf{T}_{06}$ being a hyperdiagonal matrix, suffice for the formulation of the global tangent stiffness.

4 NUMERICAL EXAMPLES

Numerical examples are presented to test and verify the efficiency of the proposed nonlinear dynamic formulation of the TRIC element. The examples are nonlinear dynamic problems that present simultaneously material and geometrical nonlinearities. The results are compared to those found in the literature and produced by the commercial code ABAQUS.

4.1 Plate with constant distributed load.

The first example examines the dynamic response of a simply supported square plate with side length L=10 in, shown in Figure 4.

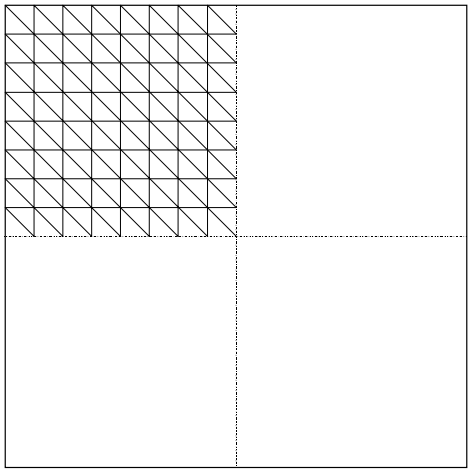

Figure 4: Simply supported square plate. Finite element discretization

The thickness of the plate is considered to be 0.5 in, the elastic modulus $E=10^7$ psi, the Poisson ratio $\nu=0.3$, the density $\rho=2.588\cdot10^{-4}$ lb·s^2/in^4. Finally, the data concerning the material nonlinearity are the yield stress $\sigma_y=30000$ psi and the plastic modulus $E_p=0$ psi.

The structure is subjected to an impulsive uniform load p=300 psi. Due to symmetry of the structure only a quarter of the plate is examined. The plate is divided by 81 vertices to 128 triangles. The dynamic response predicted by the TRIC shell element and its comparison to the solution produced by ABAQUS is presented in Figure 5. For obtaining the solution with the ABAQUS code quadrilateral elements were used since the available triangular elements of ABAQUS were not sufficiently accurate. The comparison of the results shows that the results obtained by the TRIC shell element appear to be reliable.

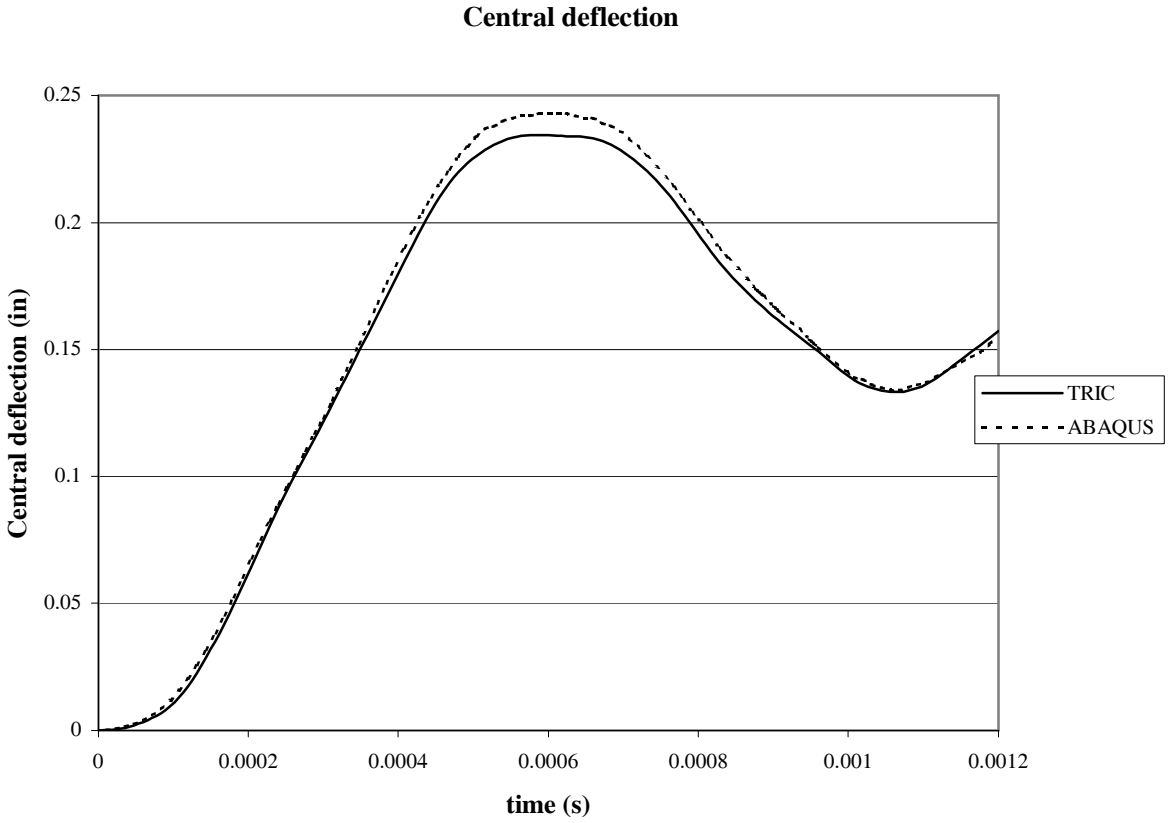

Figure 5: Central deflection of the simply supported square plate

4.2 Spherical cap under impulse loading

The second example examines the dynamic response of a spherical cap subjected to uniform impulse loading. It is an example that presents high nonlinearities in a shell structure curved along two directions. The geometry and the material properties of the structure are shown in Figure 6.

Due to symmetry of the problem only one quarter of the structure is examined. The finite element mesh used for the discretization of the structure is shown in Figure 7. It consists of 81 nodes, 128 elements and a total of 337 d.o.f..

The results produced by the TRIC shell element compared to the ones encountered in the literature are plotted in Figure 8. Again, the TRIC shell element seems to follow satisfactorily the curves obtained by other researchers[vi,vii].

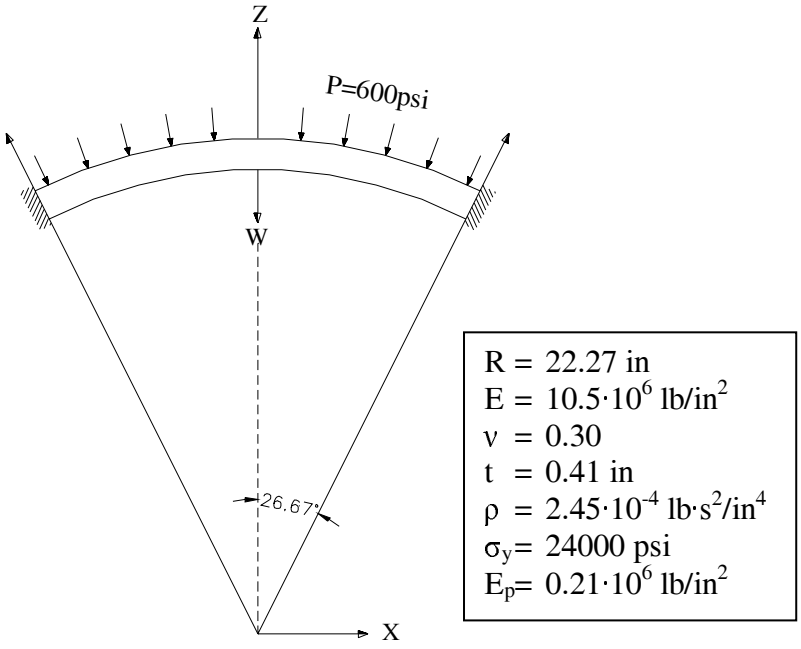

Figure 6: Spherical cap. Geometry and material properties

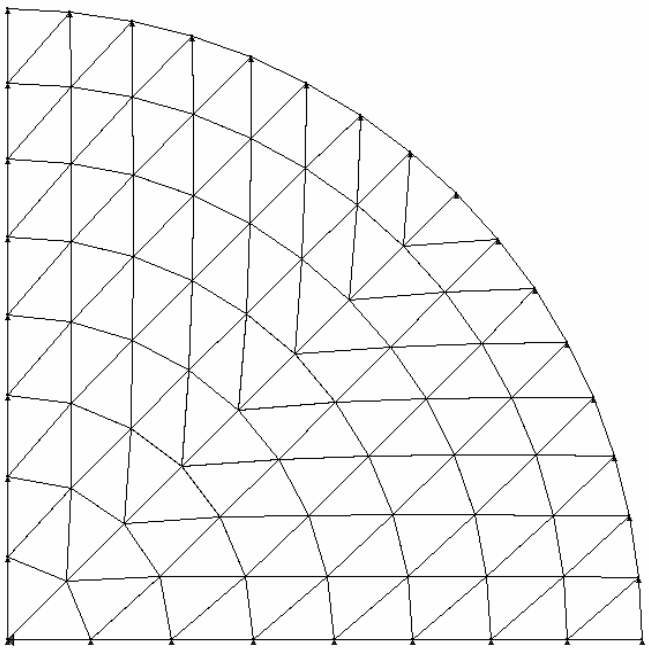

Figure 7: Spherical cap. Finite element mesh

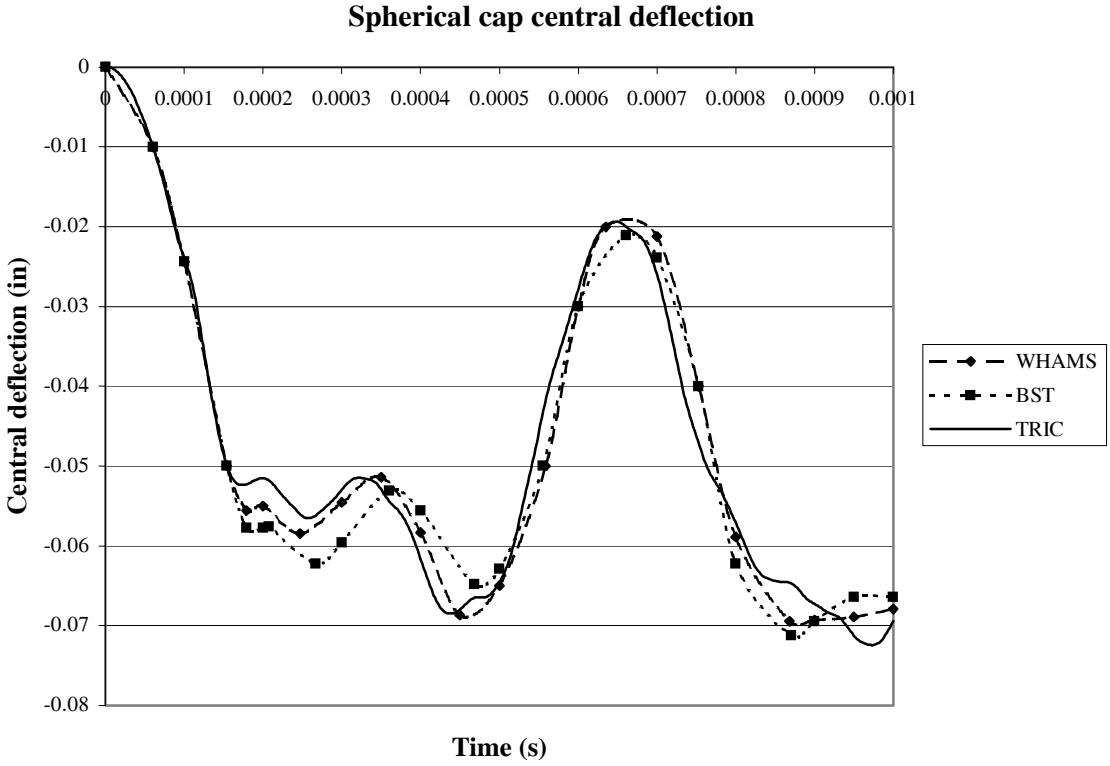

Figure 8: Spherical cap central deflection

REFERENCES

[i] J.H., Argyris, L. Tenek and L. Olofsson, "Nonlinear free vibrations of composite plates" *Comput. Methods Appl. Mech. Engrg.*, 115 (1994) 1-51.

[ii] J.H. Argyris, L. Tenek, L. Olofsson, TRIC: a simple but sophisticated 3-node triangular element based on 6 rigid body and 12 straining modes for fast computational simulations of arbitrary isotropic and laminated composite shells, Computer Methods in Applied Mechanics and Engineering 145 (1997) 11-85.

[iii] J.H. Argyris, L. Tenek, M. Papadrakakis, C. Apostolopoulou, Postbuckling performance of the TRIC natural mode triangular element for isotropic and laminated composite shells, Computer Methods in Applied Mechanics and Engineering 166 (1998) 211-231.

[iv] J.H., Argyris, M. Papadrakakis, C. Apostolopoulou and S. Koutsourelakis, "The TRIC shell element: theoretical and numerical investigation." *Comput. Methods Appl. Mech. Engrg.*, 182 (2000) 217-245.

[v] J.H. Argyris, M. Papadrakakis, L. Karapitta, Elasto-plastic analysis of shells with the triangular element TRIC, Computer Methods in Applied Mechanics and Engineering 191 (2002) 3613-3636.
[vi] E. Oñate, P. Cendoya and J. Miquel, "Non-linear explicit dynamic analysis of shells using the BST rotation-free triangle", *Engineering Computations* 19 (2002) 662-706.
[vii] WHAMS-3D, "An explicit 3D finite element program", KSB2 Inc., Willow Springs, Illinois 60480, USA.